Motor Sizing of a Ship-Mounted Two-DoF Manipulator System Considering Variations of Ocean Wave Direction

Mohamad Luthfi Ramadiansyah
Research Center for Smart Mechatronics, National Research and Innovation Agency (BRIN), Indonesia

Yazid, Edwar
Research Center for Smart Mechatronics, National Research and Innovation Agency (BRIN), Indonesia

Mirdanies, Midriem
Research Center for Smart Mechatronics, National Research and Innovation Agency (BRIN), Indonesia

Rahmat
Research Center for Smart Mechatronics, National Research and Innovation Agency (BRIN), Indonesia

他

https://doi.org/10.5109/7151721

出版情報：Evergreen. 10 (3), pp.1726-1735, 2023-09. 九州大学グリーンテクノロジー研究教育センター
バージョン：

Motor Sizing of a Ship-Mounted Two-DoF Manipulator System Considering Variations of Ocean Wave Direction

Mohamad Luthfi Ramadiansyah[1,*], Edwar Yazid[1], Midriem Mirdanies[1], Rahmat[1], Budi Azhari[1], Muhammad Fathul Hikmawan[1]

[1]Research Center for Smart Mechatronics, National Research and Innovation Agency (BRIN), Indonesia

*Author to whom correspondence should be addressed:
E-mail: moha057@brin.go.id

(Received February 20, 2023; Revised July 21, 2023; accepted July 26, 2023).

Abstract: Inverse dynamics model of the manipulator system combined with ship motions is required in order to size the electrical motor performance for ship-mounted subsystems. This study examines a sizing methodology by developing an integrated dynamical model of a two-DoF manipulator system mounted on the ship by using Lagrange-Euler method and simulating ship motions using ANSYS AQWA. Given the parameters of manipulator links and six-DoF ship motions, joint torques of a two-DoF manipulator and its electrical motors can be calculated by including the mechanical transmission. Under variations of wave direction with the JONSWAP spectrum applied, the results show that the ship motions significantly contribute to the mechanical and electrical manipulator torques, with the highest value at the 90° wave direction (beam sea) for the azimuth motor and at the 45° wave direction (quartering sea) for the elevation motor. The results can be used to size the motor torque specification by taking into account the random wave-induced ship motions and they can be extended to the development of a robust control system for the manipulator system.

Keywords: Electrical Motor, Two-DoF Manipulator, Inverse Dynamics, Lagrange-Euler, Hydrodynamics Response

1. Introduction

Robotic technology is widely used in many engineering applications, such as vehicles[1)], industrial[2)], communication[3)], underwater[4)], and humanoid robots[5)] with their own objectives. It also has been carried out by Vaibhav[6)] in the hexapod walking robot design and Himanshu[7)] for a baggage sorting robot. A manipulator system is one of the robotic applications which has several links in terms of its degrees of freedom. Kinematics and dynamics analyses are the essential tasks that need to be fulfilled in the manipulator design. It has been carried out by Chauhan and Khare[8)] for the kinematic analysis of a six-DoF industrial robot arm. Dynamic analysis is then used to obtain some dynamic parameters such as torsion, force, or acceleration of the manipulator links.

Motor sizing in the two-DoF manipulator system is a substantial phase that needs to be performed to obtain a proper motor performance. When the system is mounted on a ship and applied in the ocean, the accuracy of the manipulator's motion to lock the target position will be degraded due to unsteady ship motions. Such a condition also leads to potentially serious damage to the manipulator. To compensate ship's motions, manipulator dynamics analysis needs to take into account the ship dynamics since the ocean wave induces the ship.

The literature contains prior research on a variety of related topics. Some references are focusing on the control system, i.e. Love[9)] robot control modeling on ships, Kosuge[10)] for controlling manipulators floating on water, Kajita[11)] discussed force control of floating manipulators, and Oh[12)] designed a robust two-stage parallel cable robot controller. A dynamic model for mechanism on a non-inertial base had been addressed by applying one direction of the regular wave[13)]. Research by Hong[14)] is the closest reference to the current paper that addresses the dynamic analysis of a two-DOF manipulator subjected to regular and random waves. Preliminary research on motor sizing has been done for a manipulator system with a fixed base[15)]. However, depending on the information that the author observes, research on the ship motions that are applied to the manipulator system is relatively rare. The six-DoF ship motions are taken into account in this paper to improve the work dynamics[16)] of a two-DoF manipulator installed on a ship with different hydrodynamic processing tools and to investigate the effect of ocean wave directions. Luo found that in the offshore application of the power transmission system, the dynamics of the wire were significantly affected by the wave and wind direction[17)].

Hence, this paper's contributions are to develop a two-DoF manipulator integrated inverse dynamics model by

taking the dynamics of a ship and mechanical transmission (gearbox) system into consideration, to simulate ship motions with various ocean wave directions using commercial software ANSYS AQWA, to calculate the manipulator motor's performance while taking into account ship motions at predetermined joint angles, and to evaluate whether ocean wave direction affects motor performance.

This paper is outlined as follows: Section 2 describes the system description covering the ship geometry and the two-DoF manipulator system. Section 3 contains the research methodology. Section 4 presents the results and discussion. Section 5 provides conclusions and recommendations.

2. Description of the system

The modeling of a two-DoF manipulator system mounted on the ship tshown in Fig. 1 employs three coordinate systems. Apart from the ship, the reference coordinate frame or inertial coordinate is denoted as O_n-$X_nY_nZ_n$. The ship coordinate, which is attached to the hull and located at the center of gravity, is denoted as O_S-$X_SY_SZ_S$. It corresponds to the primary axes of the translational ship motions (surge, sway, and heave). Roll (ϕ), pitch (φ), and yaw (ψ) are rotational ship motions that rotate about the axis of a surge, sway, and heave, respectively. For details, the ship model as well as the inertial and ship coordinates are shown in Fig. 1(a). The manipulator coordinate that is applied in the manipulator system is notated as O_0-$X_0Y_0Z_0$ and follows the Denavit Hartenberg notation. It should be noted that the ship dynamics are derived at zero speed, so the inertial and ship coordinates are assumed to be a coincidence. The manipulator system is operated and placed at the ship's center of gravity (CoG), then the distance between the ship and manipulator coordinates becomes zero.

In addition, the geometrical parameters and schematic of the manipulator are shown in Fig. 1(b). The manipulator has two joints termed azimuth and elevation. The azimuth joint rotates the link in the horizontal plane with an azimuth angle (θ_{l1}) and the elevation joint rotates the link in the vertical plane with an elevation angle (θ_{l2}). Both angles will change in relation to the target position P, and a camera mounted on the manipulator is used to determine the target's position (Δ_X, Δ_Y, Δ_Z).

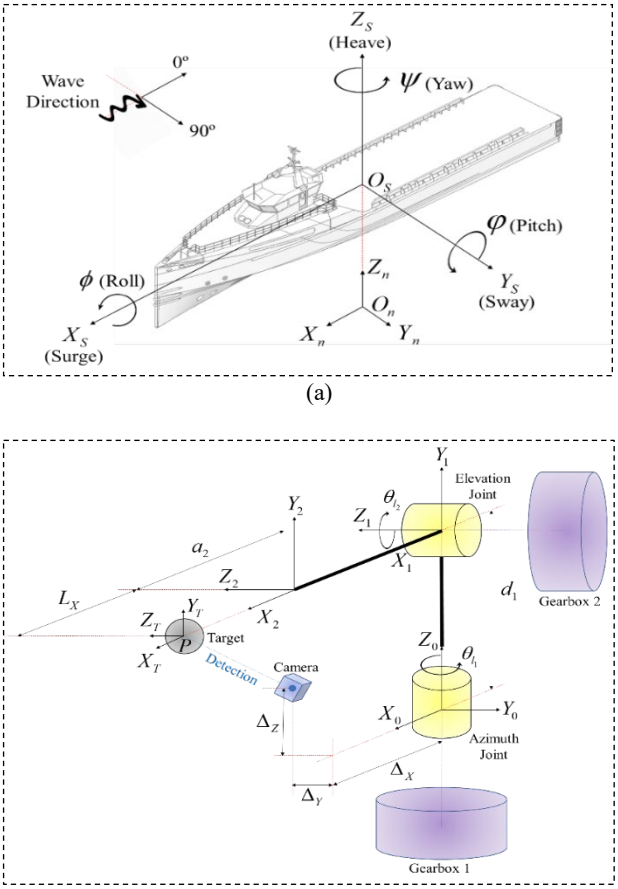

Fig. 1: Models of (a) ship and (b) two-DoF manipulator system.

3. Research methodology

The workflow for simulating the inverse dynamics model of a two-DoF manipulator mounted on the ship is depicted in Fig. 2. The electrical motor torques are derived from the inverse dynamics model with input from joint trajectories and ship motions. Each step is discussed in the next subsections.

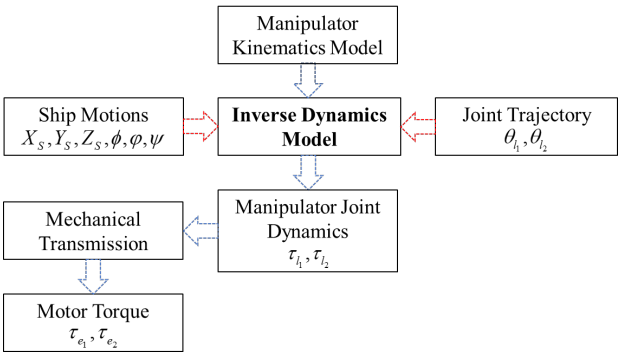

Fig. 2: Workflow for simulating the ship-mounted two-DoF manipulator's inverse dynamics.

3.1 Models of ship motions

To simulate the ship motions, ANSYS AQWA is employed to simplify the modeling process from the hull

model until the ship motions analysis. AQWA has also been widely utilized by researchers to analyze a variety of maritime and offshore structures, including wave energy dissipators[18], floating breakwaters by Samei[19] and Rajabi[20], wave energy converters[21], vessels[22], and wind turbines by Chu[23] and Huijs[24]. Steps for simulating the ship motions subjected to ocean waves inside the AQWA are visualized in Fig. 3.

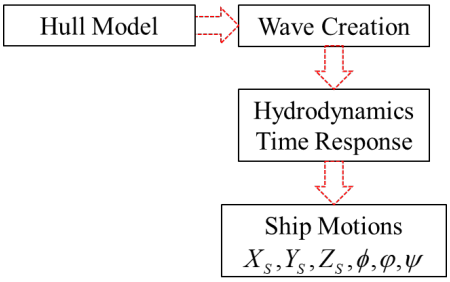

Fig. 3: Steps for simulating the ship motions subjected to ocean waves.

The 3D hull model is prepared according to the selected ship and then imported into AQWA with predefined parameters, such as the position of CoG, size of the water domain, and inertia moments of the hull. Fig. 4 depicts the ship hull model and meshing step.

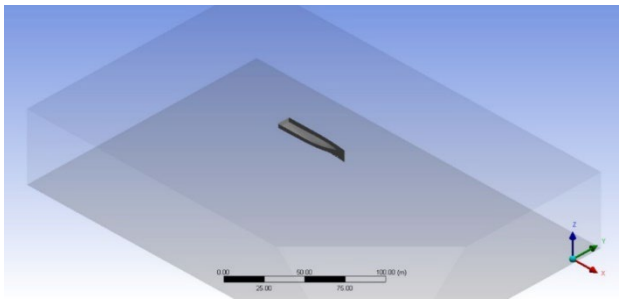

(a)

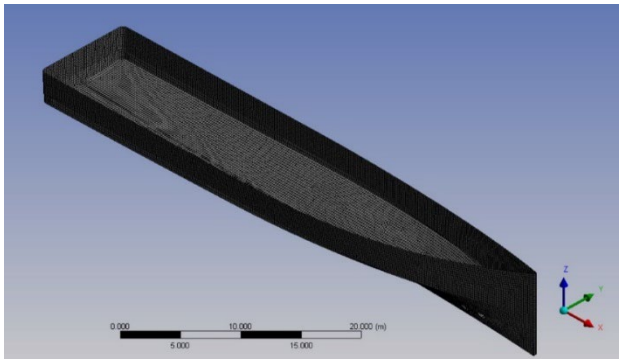

(b)

Fig. 4: Ship hull model (a) ocean boundary size (b) meshing step.

The standard ocean wave models are used in the form of a power spectrum. The spectrum that is adopted in this paper is the JONSWAP type spectrum, which is more versatile than other spectrums. This ocean wave generation is different from the free surface that has been performed by Mohd[25], where the surface generation was using Lattice Boltzmann Method[26]. The JONSWAP spectrum at a frequency (ω) is written as,

$$S(\omega) = \frac{\alpha H_s^2 \omega_p^4}{\omega^5} \exp\left[-1.25\left(\frac{\omega_p}{\omega}\right)^4\right] \gamma^b \quad (1)$$

$$b = \exp\left[-\frac{(\omega-\omega_p)^2}{2\sigma^2\omega_p^2}\right] \quad (2)$$

Eq. (1) defines the following parameters: α represents the Phillips constant, ω_p is the wave peak frequency (rad/s), H_s is the significant wave height (m), γ is the parameter of peakedness, which ranges from 1 to 7, and σ is shape parameter[27]. To generate random ocean waves, wave peak frequency, significant wave height, peakedness parameter, and wave direction must be determined.

The wave energy is converted into fluid mass flow by AQWA, and the wave impulses affect the ship's hull to move. The Hydrodynamics Time Response feature is used to process the global equation of motion, which is the basis for the numerical iteration. Simulation is defined by the time step and limit, which the hull is induced by the ocean waves. Thus, the ship motions, such as position, velocity, and acceleration, can be obtained from simulation.

3.2 Models of manipulator kinematics

There are two approaches to defining the models of manipulator kinematics: forward and inverse. As seen in Fig. 1, the manipulator kinematics model can be generated in a forward approach in terms of a homogeneous transformation matrix that refer to the Denavit Hartenberg notation. The homogeneous transformation matrix for each link can be written as,

$${}^{i-1}_{i}T_M = \begin{bmatrix} c\theta_{l_i} & -s\theta_{l_i}c\alpha_{l_i} & s\theta_{l_1}s\alpha_{l_1} & a_i c\theta_{l_1} \\ s\theta_{l_i} & c\theta_{l_1}c\alpha_{l_1} & -c\theta_{l_1}s\alpha_{l_1} & a_i s\theta_{l_1} \\ 0 & s\alpha_{l_1} & c\alpha_{l_1} & d_i \\ 0 & 0 & 0 & 1 \end{bmatrix} \quad (3)$$

$${}^{0}_{2}T_M = {}^{0}_{1}T_M \cdot {}^{1}_{2}T_M \quad (4)$$

The notations in Eq. (3) are as follows: s and c represent sin and cos, respectively; a and d are the link lengths in the X and Z axes (m); θ and α are rotational link angles in the Z and X axes (rad). From Eq. (3), it is derived sequentially from the ship (T_S), manipulator (T_M), camera (T_C), and target (T_T). The matrix is written as,

$$T = T_S \cdot {}^{2}_{0}T_M \cdot T_C \cdot T_T \quad (5)$$

The homogeneous transformation matrix of a ship is derived from the six-DoF motion and it can be expressed in Eq. (6) where matrices of T_C and T_T are excluded for the sake of simplification,

$$T_S = \begin{bmatrix} c\psi c\varphi & c\psi s\varphi s\phi - s\psi c\phi & c\psi c\phi s\varphi + s\psi s\phi & X_S \\ s\psi c\varphi & s\phi s\varphi s\psi + c\psi c\phi & s\varphi s\psi c\phi - c\psi s\phi & Y_S \\ -s\varphi & c\varphi s\phi & c\varphi c\phi & Z_S \\ 0 & 0 & 0 & 1 \end{bmatrix} \quad (6)$$

3.3 Models of inverse dynamics

The Lagrange-Euler method is used to derive an inverse dynamics model of a two-DoF manipulator system. Lagrange formulation is an energy-based approach defined as the difference between a mechanical system's kinetic energy (K) and potential energy (U). It can be written as follows,

$$L\left(\Theta,\dot{\Theta}\right) = K\left(\Theta,\dot{\Theta}\right) - U\left(\Theta\right) \quad (7)$$

Term Θ is joint position (m or rad) and $\dot{\Theta}$ is joint velocity (m/s or rad/s) of the manipulator, which can be applied to both rotational and translational motions. The kinetic energy and potential energy of the i-th link can be expressed as,

$$K_i = \frac{1}{2} m_i v_{C_i}^T v_{C_i} + \frac{1}{2} {}^i\omega_i^T \, {}^{C_i}I_i \, {}^i\omega_i \quad (8)$$

$$U_i = -m_i \, {}^0g^T \, {}^0P_{C_i} \quad (9)$$

Term P is 3 x 1 vector of position obtained from homogeneous transformation matrix. Terms m_i, v_{ci}, ω_i, and I_i represent the link's mass (kg), linear velocity (m/s), angular velocity (rad/s), and moment of inertia (kg.m^2), respectively. The velocity propagation is used to calculate linear and angular velocity of the link as follows,

$${}^{i+1}v_{i+1} = {}^{i+1}_{i}R\left({}^iv_i + {}^i\omega_i \times {}^iP_{i+1}\right) + \dot{d}_{i+1} \, {}^{i+1}\hat{Z}_{i+1} \quad (10)$$

$${}^{i+1}\omega_{i+1} = {}^{i+1}_{i}R \, {}^i\omega_i + \dot{\theta}_{i+1} \, {}^{i+1}\hat{Z}_{i+1} \quad (11)$$

Term R is 3 x 3 rotational matrix from the homogeneous transformation matrix, $\dot{d}$ is the linear velocity matrix (m/s), $\dot{\theta}$ is the angular velocity matrix (rad/s), and $\hat{Z}$ is the vector direction of the joint. Once the Lagrange equation is obtained from Eq. (7), the Euler equation is applied to form an equation of motion for the manipulator, which is written as,

$$\frac{d}{dt}\frac{\partial L}{\partial \dot{\Theta}} - \frac{\partial L}{\partial \Theta} = \tau \quad (12)$$

or it can be rewritten as,

$$\frac{d}{dt}\frac{\partial K}{\partial \dot{\Theta}} - \frac{\partial K}{\partial \Theta} + \frac{\partial U}{\partial \Theta} = \tau \quad (13)$$

Term τ is n x 1 manipulator joint torque matrix which can be separated and expressed as follows[28],

$$\tau = M\left(\Theta\right)\ddot{\Theta} + V\left(\Theta,\dot{\Theta}\right) + G\left(\Theta\right) \quad (14)$$

Term M denotes the inertia matrix n x n, V is n x 1 matrix of centrifugal and Coriolis, and G is n x 1 matrix of gravity.

3.4 Models of mechanical transmission and electrical motor

Mechanical transmission is applied to manipulate the angular velocity and torque of the electrical motor. It is located on the manipulator gearbox, as shown in Fig. 1. Schematic of mechanical transmission is depicted in Fig. 5 below.

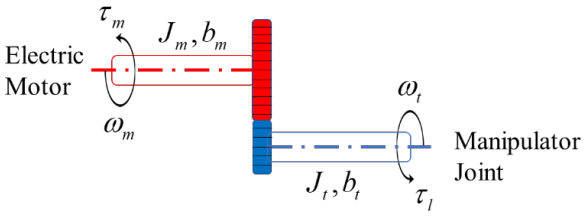

Fig. 5: Schematic of a rigid mechanical transmission.

Under static conditions and assuming that it is a rigid body[15], the torque of an electrical motor can be calculated as follows,

$$\tau_m(t) = J_m \frac{\partial \omega_m}{\partial t}(t) + b_m \, \omega_m(t) + \frac{1}{G}\tau_1(t) \quad (15)$$

$$\tau_2(t) = J_t \frac{\partial \omega_t}{\partial t}(t) + b_t \, \omega_t(t) + \frac{1}{G}\tau_\ell(t) \quad (16)$$

$$\tau_1(t)\,\omega_m(t) = \tau_2(t)\,\omega_t(t) \quad (17)$$

$$G = \frac{\omega_m(t)}{\omega_t(t)} \quad (18)$$

Term J is transmission inertia (kg.m^2), b is transmission friction (N.s/rad), and G is ratio of gear. By substituting (17) and (18) into (16), Equation (15) can be expanded and rewritten into,

$$\tau_m = \left(J_m + \frac{1}{G^2}J_t\right)\frac{\partial \omega_m}{\partial t} + \left(b_m + \frac{1}{G^2}b_t\right)\omega_m + \frac{1}{G}\tau_l \quad (19)$$

$$\tau_m = J_{eqv}\frac{\partial \omega_m}{\partial t} + B_{eqv}\,\omega_m + \frac{1}{G}\tau_\ell \quad (20)$$

By taking $\tau_m \approx \tau_e$ and $\omega_m \approx \frac{2}{P}\omega_r$, electrical torque of the motor can be expressed as,

$$\tau_e = \frac{2}{P}\left(J_{eqv}\ddot{\theta}_r\right) + \frac{2}{P}\left(B_{eqv}\dot{\theta}_r\right) + \frac{1}{G}\tau_\ell \qquad (21)$$

4. Results and discussions

The ship is subjected to random ocean waves, with its parameters shown in Table 1 and wave parameters and directions shown in Table 2. Simulations are performed in time duration of 100 s, and the results are displayed in Fig. 6. With geometry and simulation settings of the designated ship, in general, random waves with 0° direction (heading sea), amplitude of the surge motion becomes the biggest. Nevertheless, below 78 seconds in the motion responses, the pitch motion also exhibits biggest amplitude although it decreases as time increases. Further, when the ship is subject to random waves with 90° direction (beam sea), biggest amplitude is found in the sway and roll motions. However, a phenomenon in heading sea is again found that below 78 seconds, biggest amplitude is also found in the yaw motion when the random waves propagate in 45° direction (quartering sea). However, after that period, the beam sea takes over.

Joint trajectories are defined by maximum angle of azimuth of 360° and elevation of 60°. They are designed to move from 0° position to the aforementioned maximum angles continuously using a 5th-order spline function. Main parameters for two-DoF manipulator and mechanical transmission are tabulated in Table 3. The equation of motion of manipulator in Eq. (14) is then utilized which contains the dynamic terms of torque such as inertia, centripetal, Coriolis, and gravity. Predefined joint Trajectories in terms of position, velocity, and acceleration for both joint angles and the six- DoF ship motion are fed into those terms. Figure 7 presents the simulation results with an azimuth link in Fig. 7(a) and an elevation link in Fig. 7(b). As can be observed, manipulator joint torque becomes unstable (oscillation) and increases to certain maximum values when its base is disturbed by the ship motions. The beam sea produces the greatest manipulator torque in the azimuth link, where the increment is approximately 335.26 N.m. with respect to the manipulator system without ship motions. Meanwhile, in the quartering sea at 45° wave direction, the highest torque is found in the elevation link where the increment is up to 89.39 N.m.

Further investigation is conducted by comparing the torque distributions between manipulators without ship motions in Fig. 8(a) and with ship motions in Fig. 8(b) subject to beam sea based on Eq. (14). As shown in Fig.8, the gravity term is a major contributor to the elevation joint torque (bottom graph), and the inertia term is a major contributor to the azimuth joint torque (top graph).

Table 1. Ship Parameters.

Parameter	**Value**
Density of water (kg/m^3)	1025
Water domain (m)	[300; 200; 60]
Gravity (m/s^2)	9.81
Length BPP (m)	53.249
Breadth (m)	9.515
Draught (m)	3.128
Total mass (kg)	600858
Center of Gravity (CoG) (m)	[0; 0; 0]
Center of Bouyancy (CoB) (m)	[0; 0; 0.827]
Radius of gyration (m)	[3.18; 13.31; 13.85]

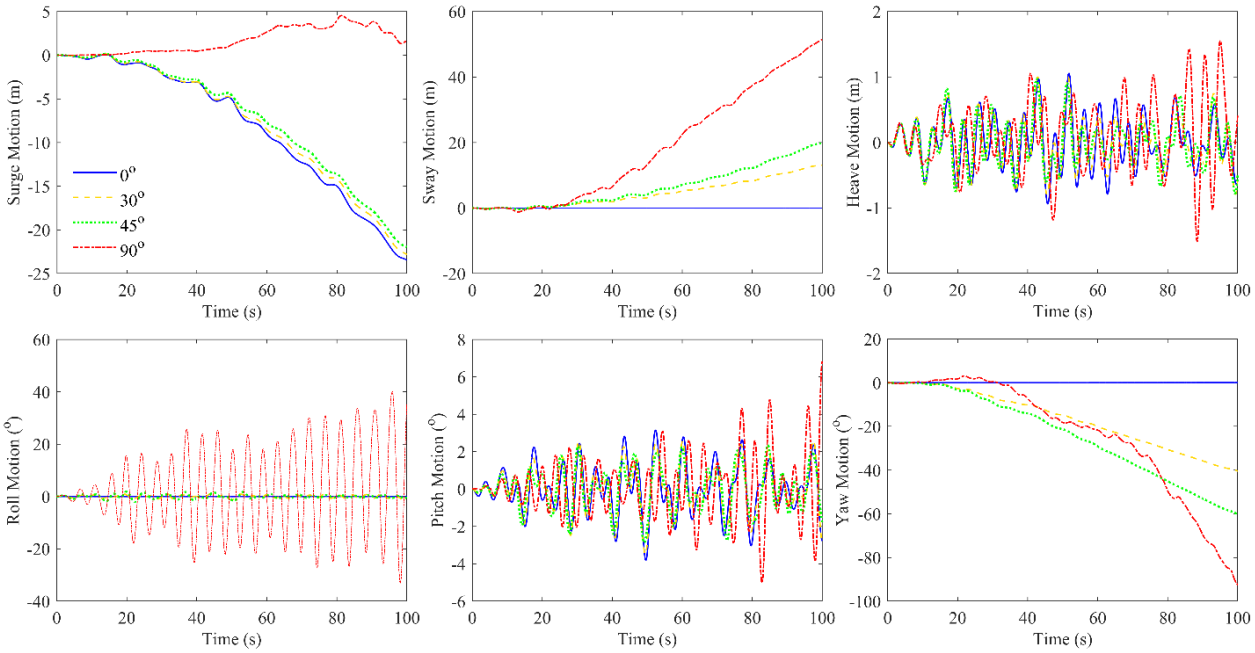

Fig. 6: Ship motions subject to variations of random ocean wave direction.

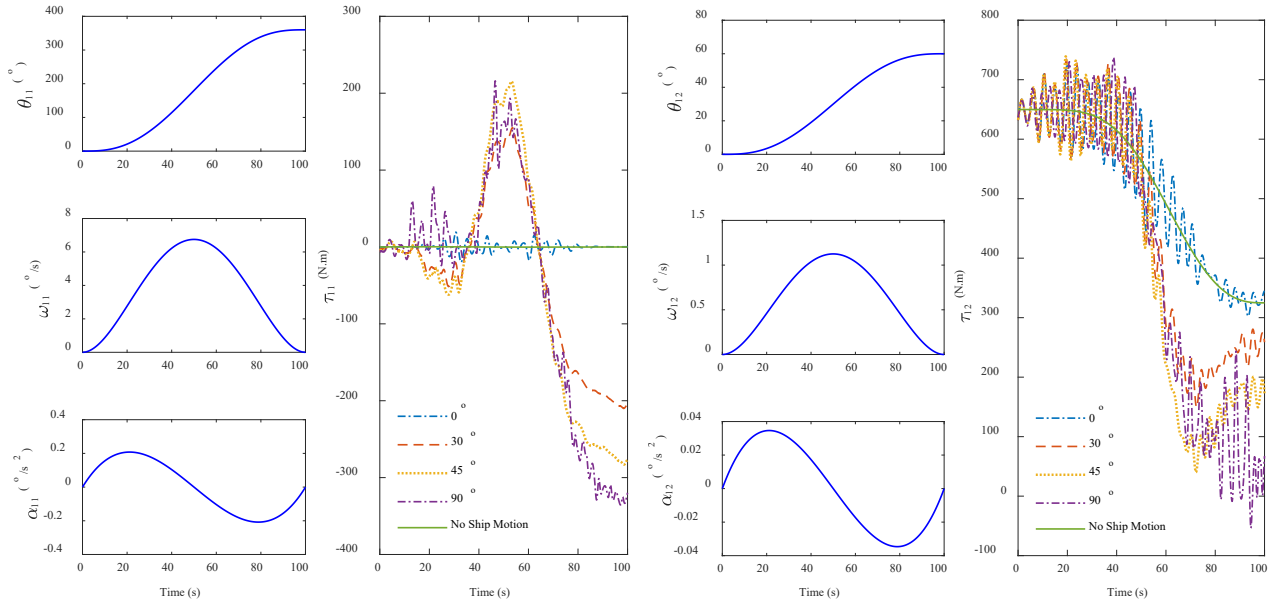

(a) (b)

Fig. 7: Manipulator torque of (a) azimuth link (b) elevation link.

Table 2. Wave Direction Series.

Wave Direction	**Sea State**	**Significant Wave Height (m)**	**Peak Frequency (Hz)**
Heading sea (0°)	Moderate	2	0.1
Quartering sea (30°)			
Quartering sea (45°)			
Beam sea (90°)			

Table 3. Two-DoF Manipulator Parameters.

Parameter	**Value**
Mass (kg)	$m_1 = 135$; $m_2 = 103.5$
CoG Position (m)	$r_{x1} = 0.00$; $r_{y1} = 0.187$; $r_{z1} = 0.00$; $r_{x2} = 0.638$; $r_{y2} = 0.453$ $r_{z2} = 0.398$
Moment of Inertia (kg.m^2)	$Ixx_1 = 4.25$; $Iyy_1 = 5.45$; $Izz_1 = 5.98$; $Ixy_1 = 0.043$; $Iyz_1 = 0.553$; $Ixz_1 = 0.012$; $Ixx_2 = 0.108$; $Iyy_2 = 14.745$; $Izz_2 = 14.74$; $Ixy_2 = 0.083$; $Iyz_2 = 0.002$; $Ixz_2 = 0.019$
Gear Ratio	$G_1 = 1$; $G_2 = 7.5$
Transmission Inertia Coef. (kg.m^2)	$J_1 = 6.528e^{-3}$; $J_2 = 5.337e^{-4}$
Transmission Friction Coef. (N.s/rad)	$b_1 = 3.572e^{-2}$; $b_2 = 3.566e^{-4}$

Azimuth joint is directly affected by the yaw motion due to it moves in the same direction as the azimuth link rotation, which is why the highest azimuth torque is achieved at beam sea. Gravity term contains pitch and yaw motions as well as the angle of elevation link. As seen in Fig. 6, the quartering sea has a higher pitch and yaw motions than the beam sea at the beginning of response. Since the elevation torque is higher at the beginning of elevation link motions, the highest torque is achieved in the 45° wave direction.

As stated in the previous section, the electrical motor torque performance is calculated from the manipulator torque in Eq. (14) through the mechanical transmission in Eq. (21) which are the results tabulated in Table 4. The electrical torque as well as the motor parameters are shown in Fig. 9(a) for azimuth and Fig. 9(b) for elevation angle. It seems that the trend is similar to that of the manipulator in Fig. 7, in which both motors oscillate with an increase in maximum torque. These findings show that the torque value can be greatly reduced by the gear ratio, but there is less contribution from the friction and inertia factors of the transmission due to joint and motor parameters being defined at a low speed. Thus, the result can be used to guide electrical motor selection in the ocean-based manipulator system.

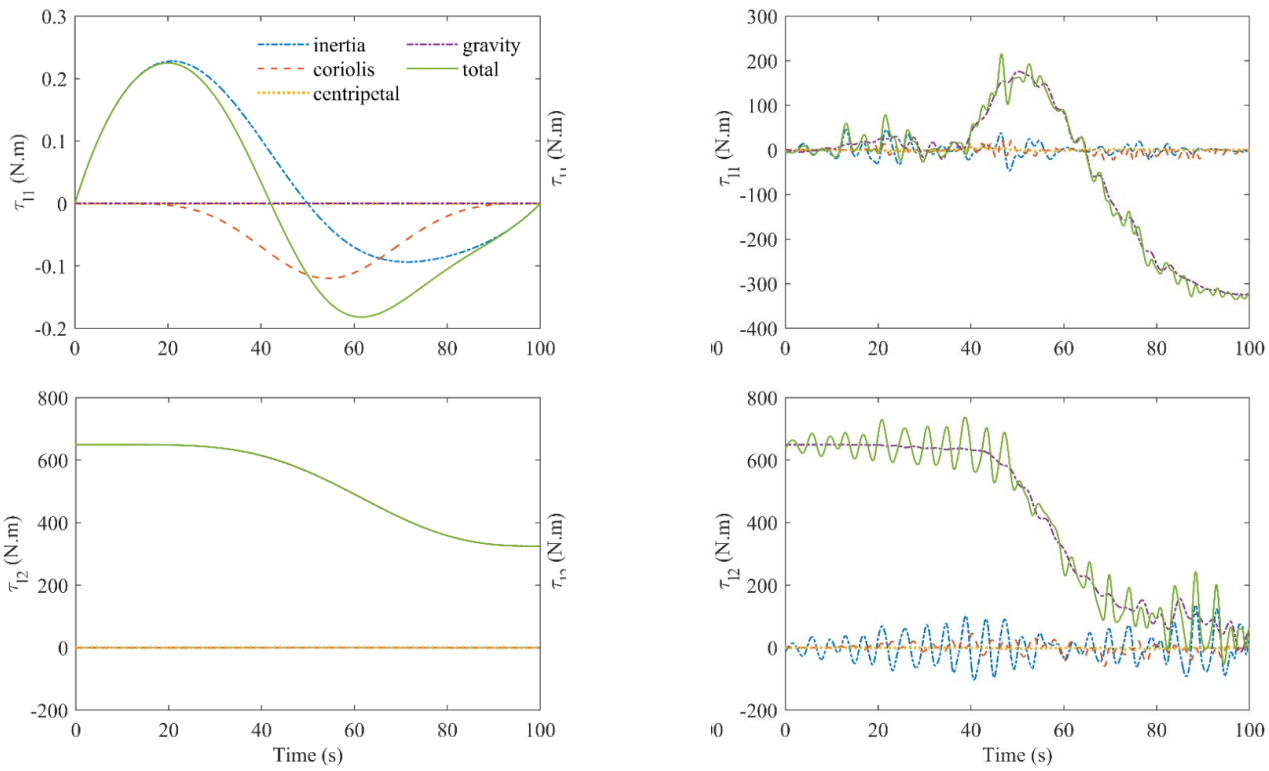

Fig. 8: Dynamics of manipulator: (a) without ship motion (b) ocean wave at 90º direction (beam sea).

Table 4. Two-DoF Manipulator Performance.

Two-DoF Manipulator	**Performance**				
	Without Ship Motions	**With Ship Motions (Direction)**			
		0º	**30º**	**45º**	**90º**
Azimuth Link	ω_{l_1} = 6.75 º/s τ_{l_1} = 0.225 N.m	ω_{l_1} = 6.75 º/s τ_{l_1} = 19.936 N.m	ω_{l_1} = 6.75 º/s τ_{l_1} = 209.949 N.m	ω_{l_1} = 6.75 º/s τ_{l_1} = 283.130 N.m	ω_{l_1} = 6.75 º/s τ_{l_1} = 335.488 N.m
Azimuth Motor	ω_{r_1} = 6.75 º/s τ_{e_1} = 0.227 N.m	ω_{r_1} = 6.75 º/s τ_{e_1} = 19.933 N.m	ω_{r_1} = 6.75 º/s τ_{e_1} = 209.949 N.m	ω_{r_1} = 6.75 º/s τ_{e_1} = 283.130 N.m	ω_{r_1} = 6.75 º/s τ_{e_1} = 335.488 N.m
Elevation Link	ω_{l_2} = 1.125 º/s τ_{l_2} = 649.831 N.m	ω_{l_2} = 1.125 º/s τ_{l_2} = 725.691 N.m	ω_{l_2} = 1.125 º/s τ_{l_2} = 734.442 N.m	ω_{l_2} = 1.125 º/s τ_{l_2} = 739.219 N.m	ω_{l_2} = 1.125 º/s τ_{l_2} = 737.635 N.m
Elevation Motor	ω_{r_2} = 8.436 º/s τ_{e_2} = 92.833 N.m	ω_{r_2} = 8.436 º/s τ_{e_2} = 103.670 N.m	ω_{r_2} = 8.436 º/s τ_{e_2} = 104.920 N.m	ω_{r_2} = 8.436 º/s τ_{e_2} = 105.603 N.m	ω_{r_2} = 8.436 º/s τ_{e_2} = 105.376 N.m

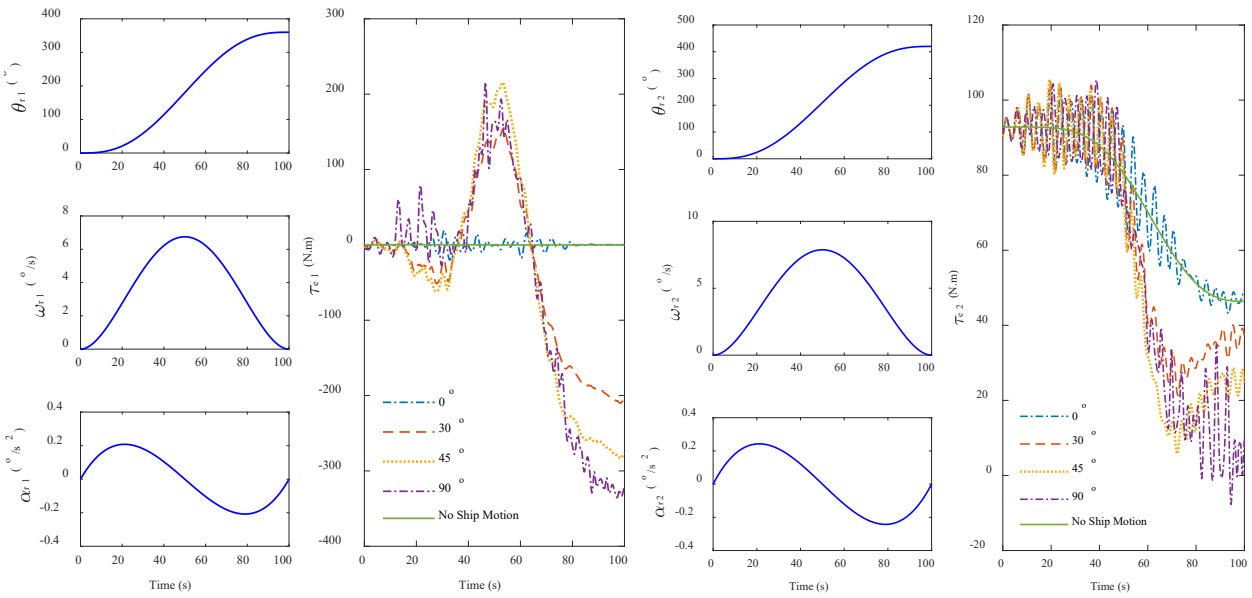

(a) (b)

Fig. 9: Electrical motor torque of (a) azimuth motor (b) elevation motor.

5. Conclusions and recommendations

Integrating the mathematical models of the ship, manipulator, and mechanical transmission enables the successful sizing of the motor employed in a ship-mounted two-DoF manipulator system. The ship motions are also successfully calculated by considering the variations of ocean wave direction. Results show that the electrical motor torque is greatly affected by the ship motions, where the value of the torque becomes higher and oscillates transiently. Ocean wave direction in the beam sea (90°) has the highest impact on the electrical torque of azimuth motor, while in the quartering sea (45°), ocean wave direction has the highest impact on the electrical torque of elevation motor. Hence, the proposed methodology and finding results in this paper can be used for sizing and selecting the electrical motor specifications that are applied to the ocean-based manipulator system. The outcome can also be used to design a reliable control system that uses an analytical methodology.

Acknowledgements

The National Research and Innovation Agency (BRIN), particularly the Research Center for Smart Mechatronics, provided the research facility, and the Ministry of Finance of the Republic of Indonesia provided financial support through the LPDP scheme with project no. PRJ-92/LPDP/2020. The authors are grateful for both of these resources.

Nomenclature

$S(\omega)$	JONSWAP spectrum (m^2 rad^{-1} s)
T	Transformation matrix (-)
K	Kinetic energy (J)
U	Potential energy (J)

Greek symbols

θ_l	Manipulator link angle (°)
θ_r	Electrical motor angle (°)
ω_l	Manipulator angular velocity (°/s)
ω_r	Electrical motor angular velocity (°/s)
α_l	Manipulator angular acceleration (°/s^2)
α_r	Electrical motor angular acceleration (°/s^2)
τ_l	Manipulator torque (N m)
τ_e	Electrical motor torque (N m)

References

1) Y. Zhao, W. Pi, W. Zhang, Q. Wang, S. Feng, H. Deng and F. Lin, "A vehicle handling inverse dynamics method for emergency avoidance path tracking based on adaptive inverse control," *IEEE Transactions on Vehicular Technology*, **70** (*6*) 5470–5482 (2021). doi:10.1109/TVT.2021.3076870.

2) N. Ramadhan, N. Lilansa, A. Rifa'i, and H. Nguyen, "Pattern recognition based movement control and gripping forces control system on arm robot model using LabVIEW," *Journal of Mechatronics, Electrical Power, and Vehicular Technology*, vol. **13** (*1*) 1–14 (2022). doi:10.14203/j.mev.2022.v13.1-14.

3) M. R. C. Qazani, H. Asadi, S. Mohamed, S. Nahavandi, J. Winter and K. Rosario, "A Real-Time Motion Control Tracking Mechanism for Satellite Tracking Antenna Using Serial Robot," in *2021*

IEEE International Conference on Systems, Man, and Cybernetics (SMC), 1049–1055 (2021), Melbourne, Australia. doi:10.1109/SMC52423.2021.9658909.

4) S. K. Deb, J. H. Rokky, T. C. Mallick and J. Shetara, “Design and construction of an underwater robot,” in *2017 4th International Conference on Advances in Electrical Engineering (ICAEE)*, 281–284 (2017), Dhaka, Bangladesh. doi:10.1109/ICAEE.2017.8255367.
5.) Z. Huang, X. Jiang, H. Liu, X. Chen, T. Fukuda and Q. Huang, “Design of crawling motion for a biped walking humanoid with 3-DoF rigid-flexible waist,” in *2018 IEEE-RAS 18th International Conference on Humanoid Robots (Humanoids)*, 974–979 (2018), Beijing, China. doi:10.1109/HUMANOIDS.2018.8624931.
6) V. Shrivastava, V. Diwakar, M. Sehgal, M. Verma and E. Neha, "Modelling and Analysis of Hexapod walking Robot," *EVERGREEN Joint Journal of Novel Carbon Resource Sciences & Green Asia Strategy*, **9** (*2*) 378-388 (2022). doi:10.5109/4794162.
7) H. Srivastava, A. Kaushal, H. Kumar, A. Tripathi and A. K. Sharma, "A Design and Development of Baggage Sorting Robotic System at the Airport," *EVERGREEN Joint Journal of Novel Carbon Resource Sciences & Green Asia Strategy*, **9** (*1*) 86-92 (2022). doi: 10.5109/4774219.
8) S. S. Chauhan and A. K. Khare, "Kinematic Analysis of the ABB IRB 1520 Industrial Robot Using RoboAnalyzer Software," *EVERGREEN Joint Journal of Novel Carbon Resource Sciences & Green Asia Strategy*, **7** (*4*) 510-518 (2020). doi:10.5109/4150470.
9) L. J. Love, J. F. Jansen and F. G. Pin, "On the modeling of robots operating on ships," *IEEE International Conference on Robotics and Automation, 2004. Proceedings. ICRA '04*, **3** 2436-2443 (2004), New Orleans, LA, USA. doi:10.1109/ROBOT.2004.1307426.
10) K. Kosuge, T. Fukuda and H. Ohkubo, "Control of manipulator/vehicle system floating on the water," *[1991] Proceedings of the 30th IEEE Conference on Decision and Control*, **3** 2781-2786 (1991), Brighton, UK. doi:10.1109/CDC.1991.261864.
11) H. Kajita and K. Kosuge, "Force control of robot floating on the water utilizing vehicle restoring force," *Proceedings of the 1997 IEEE/RSJ International Conference on Intelligent Robot and Systems. Innovative Robotics for Real-World Applications. IROS '97*, **1** 162-167 (1997), Grenoble, France. doi:10.1109/IROS.1997.649038.
12) S. R. Oh, K. Mankala, S. Agrawal and J. Albus, “Dynamic modeling and robust controller design of a two-stage parallel cable robot,” *IEEE International Conference on Robotics and Automation*, **4** 3678–3683 (2004), New Orleans, LA, USA. doi:10.1109/ROBOT.2004.1308830.
13) P. J. From, V. Duindam, J. T. Gravdahl and S. Sastry, "Modeling and motion planning for mechanisms on a non-inertial base," *2009 IEEE International Conference on Robotics and Automation*, 3320-3326 (2009), Kobe, Japan. doi:10.1109/ROBOT.2009.5152666.
14) K. S. Hong and Q. H. Ngo, “Dynamics of the container crane on a mobile harbor,” *J. Ocean Engineering*, **53** 16-24 (2012). doi:10.1016/j.oceaneng.2012.06.013.
15) E. Yazid, R. Ristiana, M. Mirdanies, R. A. Ardiansyah, R. Rahmat and Y. Sulaeman, "Sizing the Mechanical and Electrical Performances of a Two-DoF Manipulator Design Taking into Account PMSM Type Three-Phase AC Servo Motor," *2021 International Conference on Computer Science and Engineering (IC2SE)*, 1-9 (2021), Padang, Indonesia. doi:10.1109/IC2SE52832.2021.9792074.
16) E. Yazid, A. S. Nugraha, H. M. Saputra and Rahmat, "Dynamics of a Ship-Mounted Two-DoF Manipulator Case: Effect of Sea State to the Manipulator Joint Torque," *2019 IEEE International Conference on Industry 4.0, Artificial Intelligence, and Communications Technology (IAICT)*, 1-6 (2019), Bali, Indonesia. doi:10.1109/ICIAICT.2019.8784860.
17) R. Luo, H. Zhu and C. Hu, "A Numerical Investigation of an Offshore Overhead Power Transmission System," *EVERGREEN Joint Journal of Novel Carbon Resource Sciences & Green Asia Strategy*, **9** (*3*) 636-644 (2022). doi:10.5109/4842521.
18) J. C. Park, C. M. Wang and I. H. Cho, "Hydrodynamic behaviour of floating polygonal compound platforms with wide porous media," *Ocean Engineering*, **265** 112672 (2022). doi:10.1016/j.oceaneng.2022.112672.
19) S.R. Samei, F. Azarsina and M. A. Ghahferokhi, " Numerical Simulation of Floating Pontoon Breakwater with ANSYS AQWA Software and Validation of the Results with Laboratory Data," *Bulletin de la Société Royale des Sciences de Liège*, **85** 1487 - 1499 (2016). doi:10.25518/0037-9565.6194.
20) M. Rajabi and H. Ghassemi, "Hydrodynamic Performance Improvement of Double-Row Floating Breakwaters by Changing the Cross-Sectional Geometry," *Mathematical Problems in Engineering*, **2021** 2944466 (2021). doi:10.1155/2021/2944466.
21) H. Behzad and R. Panahi, "Optimization of bottom-hinged flap-type wave energy converter for a specific wave rose," *Journal of Marine Science and Application*, **16** 159–165 (2017).

doi.org:10.1007/s11804-017-1405-y.

22) R. B. Luhulima, D. Setyawan and I. Utama. "Selecting monohull, catamaran and trimaran as Suitable passenger vessels based on stability and seakeeping criteria," *Proceedings of the 14Th International Ship Stability Workshop*, 262-266 (2014), Kuala Lumpur, Malaysia.
23) Y. I. Chu and C. M. Wang, "Hydrodynamic Response Analysis of Combined Spar Wind Turbine and Fish Cage for Offshore Fish Farms," *International Journal of Structural Stability and Dynamics*, **20** 09 (2020). doi:10.1142/S0219455420501047.
24) F. Huijs, R. de Bruijin and F. Savenije, "Concept Design Verification of a Semi-submersible Floating Wind Turbine Using Coupled Simulations," *Energy Procedia*, **53** 2-12 (2014). doi:10.1016/j.egypro.2014.07.210.
25) N. Mohd, M. M. Kamra, M. Sueyoshi and C. Hu, "Three-dimensional Free Surface Flows Modeled by Lattice Boltzmann Method: A Comparison with Experimental Data," *EVERGREEN Joint Journal of Novel Carbon Resource Sciences & Green Asia Strategy*, **4 (***1*) 29-35 (2017). doi:10.5109/1808450.
26) N. Mohd, M. M. Kamra, M. Sueyoshi and C. Hu, " Lattice Boltzmann Method for Free Surface Impacting on Vertical Cylinder: A Comparison with Experimental Data," *EVERGREEN Joint Journal of Novel Carbon Resource Sciences & Green Asia Strategy*, **4 (***02/03*) 28-37 (2017). doi:10.5109/1929662.
27) K. Hasselmann, T. Barnett, E. Bouws, H. Carlson, D. E. Cartwright, K. Enke, J. A. Ewing, H. Gienapp, D. E. Hasselmann, P. Kruseman, A. Meerburg, P. Muller, D. J. Olbers, K. Richter, W. Sell and H. Walden, “Measurements of wind-wave growth and swell decay during the Joint North Sea Wave Project (JONSWAP),” Deut. Hydrogr. Z., **8** 1–95, (1973).
28) B. Siciliano, L. Sciavicco, L. Villani and G. Oriolo, "Robotics: Modelling, Planning and Control," Springer, London, 2009. https://link.springer.com/book/10.1007/978-1-84628-642-1.